LETTERS

Fault zone fabric and fault weakness

Cristiano Collettini[1], André Niemeijer[2]†, Cecilia Viti[3] & Chris Marone[2]

Geological and geophysical evidence suggests that some crustal faults are weak[1–6] compared to laboratory measurements of frictional strength[7]. Explanations for fault weakness include the presence of weak minerals[4], high fluid pressures within the fault core[8,9] and dynamic processes such as normal stress reduction[10], acoustic fluidization[11] or extreme weakening at high slip velocity[12–14]. Dynamic weakening mechanisms can explain some observations; however, creep and aseismic slip are thought to occur on weak faults, and quasi-static weakening mechanisms are required to initiate frictional slip on mis-oriented faults, at high angles to the tectonic stress field. Moreover, the maintenance of high fluid pressures requires specialized conditions[15] and weak mineral phases are not present in sufficient abundance to satisfy weak fault models[16], so weak faults remain largely unexplained. Here we provide laboratory evidence for a brittle, frictional weakening mechanism based on common fault zone fabrics. We report on the frictional strength of intact fault rocks sheared in their *in situ* geometry. Samples with well-developed foliation are extremely weak compared to their powdered equivalents. Micro- and nanostructural studies show that frictional sliding occurs along very fine-grained foliations composed of phyllosilicates (talc and smectite). When the same rocks are powdered, frictional strength is high, consistent with cataclastic processes. Our data show that fault weakness can occur in cases where weak mineral phases constitute only a small percentage of the total fault rock and that low friction results from slip on a network of weak phyllosilicate-rich surfaces that define the rock fabric. The widespread documentation of foliated fault rocks along mature faults in different tectonic settings and from many different protoliths[4,17–19] suggests that this mechanism could be a viable explanation for fault weakening in the brittle crust.

Laboratory measurements on a wide variety of rock types show that fault friction μ is in the range 0.6–0.8, independent of rock type, with the exception of a few weak minerals[7]. Several lines of evidence suggest that Byerlee's friction with $\mu = 0.6$ is applicable to many faults within the brittle crust[20], including *in situ* stress measurements showing that failure occurs on optimally oriented faults with normal friction and nearly hydrostatic pore pressure[21]. Moreover, the absence of moderate-to-large earthquakes along severely misoriented faults in both extensional and compressional environments is consistent with laboratory friction values[22]. In contrast, a number of studies have suggested that some mature crustal faults are weak compared to laboratory friction values[1–6,8,9]. Dynamic weakening mechanisms may explain some of these data. High speed friction experiments have shown that friction decreases above a threshold slip rate[12–14] and such weakening is consistent with observations of dynamic rupture[10,11,23]. However, a number of observations indicate that fault creep, aseismic slip and slip on unfavourably oriented faults with respect to the applied stress occur at low resolved shear stress, which implies that some faults are statically weak[1–4,6,8,9], that is, friction is low in the long term including both co-seismic and inter-seismic phases.

To investigate the role of fabrics in long term fault weakening, we conducted friction experiments on fault rocks obtained from the Zuccale fault, which is a low-angle normal fault exposed on the Isle of Elba (Fig. 1) in central Italy. Geological data suggest that the Zuccale fault has accommodated a total shear displacement of 6–8 km along a dip angle of about 15° in a stress field with a vertical maximum compression; that is, the fault was weak[24]. The fault zone is characterized by a foliated and lithologically heterogeneous fault core several metres thick. The adjacent hangingwall and footwall rocks deformed predominantly by brittle cataclastic processes. Within the fault core, however, a significant amount of deformation was accommodated within highly foliated phyllosilicate-rich horizons that represent deformation processes that occurred at less than 8 km of crustal depth[24]. The foliated microstructure probably formed in the early geological stages of fault activity by dissolution and precipitation processes. Once formed, the phyllosilicate-rich network deforms predominantly by frictional sliding along the phyllosilicate foliae[24].

We chose rock samples from two foliated zones (Fig. 1) for detailed friction studies (see Methods). Zone L2 is composed of massive calcite-rich portions and calcite sigmoids dispersed within a fine-grained ($<2\,\mu m$) foliation made of tremolite and phyllosilicate (smectite, talc and minor chlorite). Zone L3 contains both large crystals of calcite and agglomeration of tremolite fibres in random orientation, within a foliation made of fine-grained tremolite and phyllosilicates (smectite, talc and minor chlorite). We collected undisturbed samples of the fault rocks and cut them into wafers 0.8–1.2 cm thick and 5 cm × 5 cm in area. We refer to these as solid experiments. We also carried out experiments on powders obtained from crushing and sieving ($<150\,\mu m$) the solid samples. With this approach we directly compare the frictional properties of foliated fault rocks and their powdered equivalents, which have identical mineralogical composition (Table 1).

Frictional sliding experiments were carried out in the double direct shear configuration (Fig. 2a inset) at 25 °C and over a range of normal stresses from 10 to 150 MPa and shear slip velocities of 1 to 300 $\mu m\,s^{-1}$ (see Methods). All experiments are characterized by an initial strain hardening, where the shear stress increases rapidly during elastic loading, before a yield point, followed by shear at a steady-state value of frictional stress (Fig. 2a). We measured the steady state, residual, frictional shear stress for intact fault rocks and powders at each normal stress. Each rock type plots along a line consistent with a brittle failure envelope (Fig. 2b), but the solid wafers are much weaker than their powdered analogues. In particular, the powders show friction of about 0.6, whereas the foliated rocks have significantly lower values (0.45–0.20). We note that at each normal stress, foliated fault rocks have a friction coefficient that is 0.2–0.3 lower than the powders made from them (Fig. 3). The majority of our experiments were conducted

[1]Geologia Strutturale e Geofisica, Dipartimento di Scienze della Terra Università degli Studi di Perugia, 06100, Perugia, Italy. [2]Department of Geosciences and Energy Institute Center for Geomechanics, Geofluids, and Geohazards, Penn State University, University Park, Pennsylvania 16802, USA. [3]Dipartimento di Scienze della Terra Università degli Studi di Siena, 53100, Siena, Italy. †Present address: Istituto Nazionale di Geofisica e Vulcanologia, 00143, Roma, Italy.

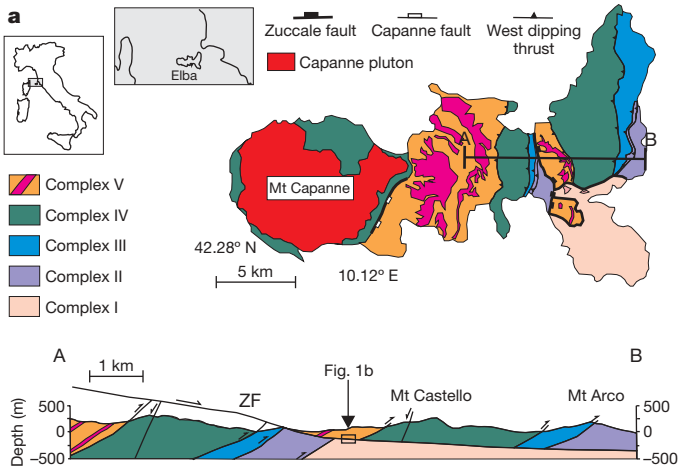

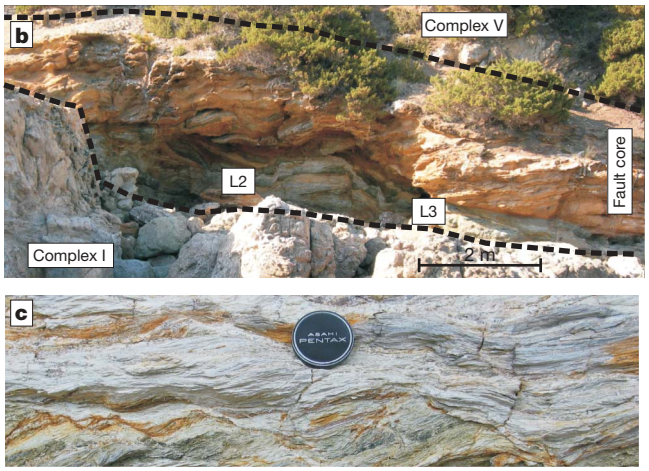

Figure 1 | Example of a foliated low-angle normal fault. **a**, Map and cross-section of the Zuccale fault (ZF) as exposed on the Isle of Elba, Central Italy. The Zuccale fault is an exhumed, ancient low-angle normal fault belonging to the Apenninic system. In the tectonically active area of the Apennines, to the east, a similar low-angle normal fault is producing microseismicity at depths[3] of 4–16 km. The geological cross-section AB through central and eastern Elba highlights the low-angle geometry[24]. **b**, Outcrop photograph of the fault structure and locations of zones L2 and L3 where samples were collected. **c**, Detail of the foliated fault rock in L2. (Camera lens cap shown for approximate scale; diameter 4 cm.)

without water and at room temperature, but we also ran experiments under water-saturated conditions and these indicate further weakening for intact fault rocks (for example, Fig. 3).

Microstructural studies of the tested rocks show that the sliding surfaces of the foliated solid wafers are located along the pre-existing very-fine-grained foliation made of tremolite and phyllosilicates (Fig. 4a and c). Transmission electron microscope (TEM) images show that the foliation is made of tremolite clasts surrounded by an interconnected network of phyllosilicates, including smectite and talc (Fig. 4e and f). The through-going microstructure is affected by translation and rotation of the (001) phyllosilicate layers with frequent interlayer delaminations, resulting in talc grain size reduction, down to 20 nm in thickness. This anastomosing network of phyllosilicate lamellae appears to provide a multitude of possible slipping planes for frictional shear under a low stress. In contrast, our experiments conducted on powder composed of the same materials indicate that much of the deformation occurs along zones characterized by grain-size reduction and affected by shear localization along R1, Y and B shears (Fig. 4b, for example[25,26]). The slipping zones of powdered samples are characterized by abundant calcite clasts immersed in a groundmass consisting of fine-grained tremolite and subordinate phyllosilicates (Fig. 4d).

Although the foliated wafers of intact fault rock and their powders have identical mineralogical compositions, the foliated samples are much weaker than their powdered analogues. On the basis of microstructural studies, we propose that weakness of the foliated fault rocks is due to the reactivation of pre-existing fine-grained and phyllosilicate-rich surfaces that are absent in the powders. The slightly higher friction coefficient of fault zone L2 compared to L3 (0.31 versus 0.25) is probably due to the presence of foliation-perpendicular calcite-filled fractures that reduce the interconnectivity of the microstructure. The frictional strength of the solid wafers is comparable to that of pure talc at similar sliding conditions[16] even with the presence of 65–80% of strong calcite and tremolite minerals up to

Table 1 | Experimental details and mineral composition of the rocks tested.

Experiment	Sample	Normal stress (MPa)	Mineralogy (%)				
			Calcite	Tremolite	Smectite	Talc	Chlorite
P2045	Wafer L2	10; 20; 35; 50	43	36	14	6	1
P2048	Wafer L3	10; 20; 35; 50	39	26	19	15	1
P2049	Powder L3	10; 20; 35; 50	39	26	19	15	1
P2050	Powder L3	75;100;150	39	26	19	15	1
P2052	Wafer L3	75;100;150	39	26	19	15	1
P2053	Wafer L2	75;100;150	43	36	14	6	1
P2054	Wafer L2	10; 20; 35; 50	43	36	14	6	1
P2056	Powder L2	10; 20; 35; 50	43	36	14	6	1
P2057	Wafer-wet L2	10; 20; 35; 50	43	36	14	6	1
P2066	Powder L2	75;100;150	43	36	14	6	1

Mineral abundances were evaluated by TG-MS and XRPD (see Methods and Supplementary Fig. 1).

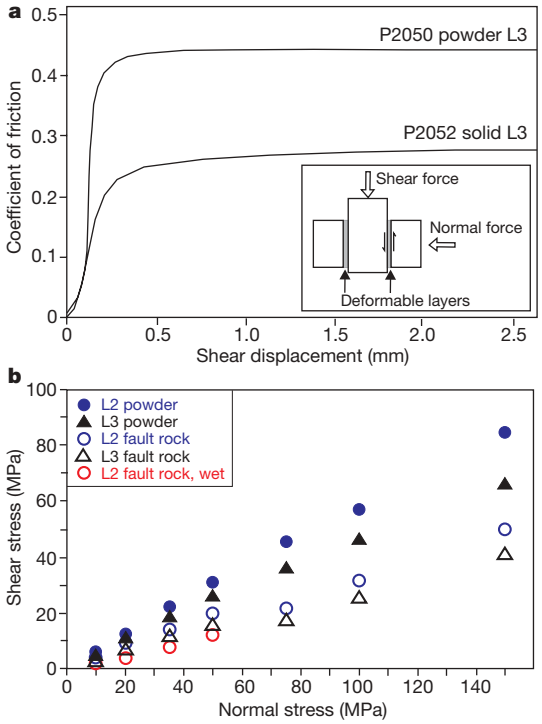

Figure 2 | Friction experiments. **a**, The inset shows the double-direct shear geometry used to shear solid and powdered samples of fault rock. The main plot shows the coefficient of friction μ versus shear displacement at the layer boundaries for a representative experiment at a normal stress of 150 MPa (sample L3). Strain hardening occurs initially, after which friction reaches a steady-state value. We note that sliding friction is significantly lower for the solid sample than for its powdered equivalent. **b**, Steady-state shear strength, measured during frictional sliding, plotted as a function of normal stress. Data for layers of powdered rock plot along lines with slopes $\mu = 0.55$ and $\mu = 0.43$ for L2 and L3 respectively. Data for shear of solid fault rock plot along lines with slopes $\mu = 0.31$ and $\mu = 0.25$ for L2 and L3 respectively.

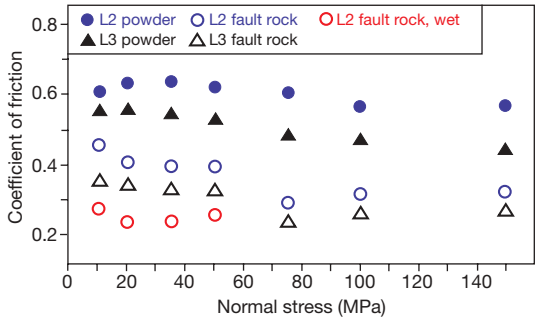

Figure 3 | Frictional properties of fault rocks and powders made from them. Steady-state friction plotted as a function of normal stress. The solid samples show friction values that are consistently 0.2–0.3 weaker than powders. Further weakening for intact fault rocks is achieved under water-saturated conditions.

200 μm wide (Table 1). This suggests that weak fault rocks can form with even small amounts of phyllosilicates as long as they form an interconnected, through-going foliated network. Although our experiments show that further weakening along phyllosilicate-rich rocks can be achieved by (1) the presence of fluids within the fault zone and (2) slow sliding velocities, the average value of $\mu = 0.25$ from our dry experiments at room temperature is sufficient to explain the absence of measurable heat flow along weak faults and frictional reactivation of faults oriented up to 75° from the maximum compressive stress, like the San Andreas or the low-angle normal faults of the Apennines.

In the core of ancient exhumed fault zones, where much of the deformation is accommodated, geological observations suggest that pervasive fluid influx can facilitate the dissolution of strong minerals and the precipitation of weak and fine-grained secondary phases[2,6,17,24,27]. With incremental shearing, these weak phyllosilicates can align to form a foliation that ultimately results in an interconnected network that allows slip to be accommodated along the weak foliation and reduces the frictional strength of the fault zones[2,6,17,24,27]. These observations have been confirmed in laboratory experiments using rock analogue materials where the combination of fluid-assisted deformation and the development of a phyllosilicate foliation at low sliding velocities and high shear strains caused major weakening of the experimental fault gouge (a decrease in μ from 0.8 to 0.25)[28,29]. Here, by performing frictional sliding experiments on intact wafers of natural fault rocks with a pre-existing phyllosilicate-rich foliation, we have demonstrated that the presence of a phyllosilicate foliation in fault zones results in significant fault weakening.

One important question involves whether fault weakening via fabric development in phyllosilicate rich rocks rules out earthquake-like frictional instability. Previous works have noted the tendency for weak materials to exhibit inherently stable frictional slip[15,16,26]. However, geological investigations have documented the mutual superposition between slip on phyllosilicates and brittle (hydrofractures) or earthquake-related structures (pseudotachylytes)[30]. Sharp and continuous slip zones of highly sheared clay-rich fault gouge have been interpreted as seismogenic principal displacement zones[13]. Continuous strands of phyllosilicates usually bound lenses of stronger lithologies[18,19]: these lenses could represent sites for stress concentrations and earthquake nucleation near patches of fault creep[18,23,31]. In addition, laboratory experiments on gouge mixtures show that when the phyllosilicates constitute a small percentage of the fault (10–30%), velocity-weakening behaviour is favoured at higher slip velocities[29,31]. A similar weak and velocity-weakening behaviour has been documented for smectite clay at low normal stress[32] (<30 MPa) and for clay-rich fault gouge in high-velocity friction experiments[14]. In this view, some crustal faults can behave as weak structures over long timescales (millions of years) and be intermittently seismogenic on shorter timescales.

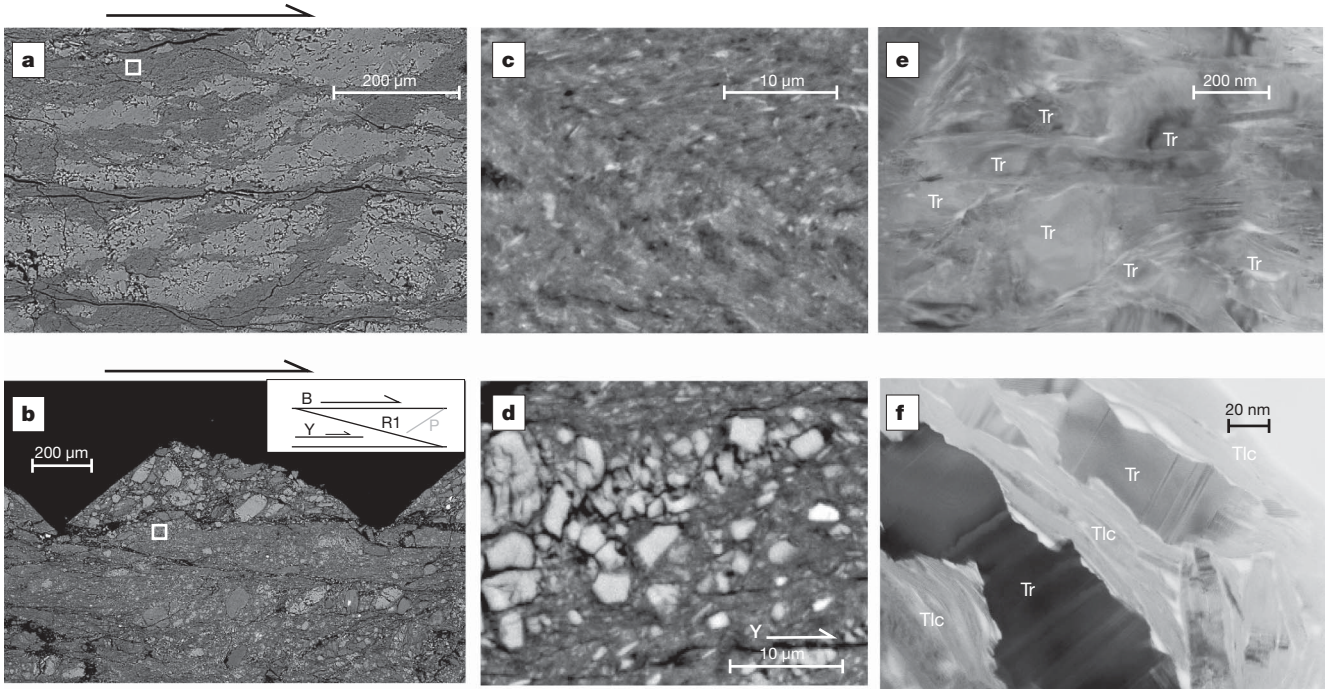

Figure 4 | Comparison between solid-foliated and powder sliding surfaces in L3. **a**, **c**, Solid experiment (P2048), total shear displacement of ~25 mm, steady friction coefficient $\mu = 0.32$. The calcite sigmoids are interdispersed within a fine-grained foliation (see detail in **c**) made of tremolite and phyllosilicates (smectite, chlorite and talc). The slipping processes occur along planes localized within the foliation. **b**, **d**, Powder experiment (P2049), total shear displacement ~25 mm, steady friction coefficient $\mu = 0.53$. The fault rock shows a cataclastic texture with zones affected by grain-size reduction (see detail in **d**) and shear localization along the R1, Y and B sliding surfaces. The little boxes in **a** and **b** represent the areas of **c** and **d**, respectively. The half arrows above **a** and **b** show direction of shear. **a**–**d** are scanning electron microscopy back-scattered electron images. **e**, **f**, TEM images, showing details of the foliated microstructure (solid experiment P2048) that is made of an interconnected network of thin, oriented phyllosilicates (smectite and talc; low-contrast portions) surrounding tremolite fibres. Tr, tremolite; Tlc, talc.

We show that fault weakening depends strongly on rock fabric and the distribution of weak phases within a fault zone. The result is akin to findings from studies involving dissolution[6] and ductile deformation[33]. However, we show that fabric-induced weakening can occur in the cataclastic, brittle deformation regime via frictional processes. Previous works focused on brittle fault strength have looked primarily at homogeneous mineral mixtures and bulk composition of the fault zone. Fluid–rock interactions and the growth of interconnected, phyllosilicate-rich networks have been documented in a wide variety of rock types[4,17–19,24,27,30]. We therefore propose that frictional sliding along such rock fabrics may be a viable mechanism to explain the mechanics of weak faults within the brittle crust.

METHODS SUMMARY

To determine the mineralogical composition of the fault rocks (Table 1), we have quantitatively combined results from X-ray powder diffraction (XRPD) and thermo-gravimetry/mass spectrometry (TG-MS) studies.

For friction experiments we collected large blocks of foliated fault rocks pertaining to L2 and L3 domains and we cut them to form wafers 0.8–1.2 cm thick and 5 cm × 5 cm in area. The wafers were oriented so that they could be sheared in their *in situ* orientation, with foliation parallel to shear direction. We refer to these as solid experiments. We also carried out experiments on powders obtained from crushing and sieving the solid wafers. Experiments were conducted in a servo-controlled biaxial deformation apparatus[16,26] (Fig. 2a inset), at room temperature and over a range of shear slip velocities from 1 to 300 $\mu m\,s^{-1}$. Data reported on Figs 2 and 3 refer to a sliding velocity of 10 $\mu m\,s^{-1}$.

Full Methods and any associated references are available in the online version of the paper at www.nature.com/nature.

Received 4 May; accepted 12 October 2009.

1. Zoback, M. D. *et al.* New evidence on the state of stress of the San Andreas fault system. *Science* **238,** 1105–1111 (1987).
2. Holdsworth, R. E. Weak faults—rotten cores. *Science* **303,** 181–182 (2004).
3. Chiaraluce, L., Chiarabba, C., Collettini, C., Piccinini, D. & Cocco, M. Architecture and mechanics of an active low-angle normal fault: Alto Tiberina Fault, northern Apennines, Italy. *J. Geophys. Res.* **112,** B10310, doi:10.1029/2007JB005015 (2007).
4. Moore, D. E. & Rymer, M. Talc-bearing serpentinites and the creeping section of the San Andreas fault. *Nature* **448,** 795–797, doi:10.1038/nature06064 (2007).
5. Brune, J. N., Henyey, T. L. & Roy, R. F. Heat flow, stress, and rate of slip along the San Andreas Fault, California. *J. Geophys. Res.* **74,** 3821–3827 (1969).
6. Wintsch, R. P., Christoffersen, R. & Kronenberg, A. K. Fluid-rock reaction weakening of fault zones. *J. Geophys. Res.* **100,** 13021–13032 (1995).
7. Byerlee, J. D. Friction of rocks. *Pure Appl. Geophys.* **116,** 615–629 (1978).
8. Rice, J. R. in *Fault Mechanics and Transport Properties of Rocks* (eds Evans, B. & Wong, T.-f.) 475–503 (Academic Press, 1992).
9. Faulkner, D. R., Mitchell, T. M., Healy, D. & Heap, M. J. Slip on 'weak' faults by the rotation of regional stress in the fracture damage zone. *Nature* **444,** 922–925 (2004).
10. Ampuero, J.-P. & Ben-Zion, Y. Cracks, pulses and macroscopic asymmetry of dynamic rupture on a bimaterial interface with velocity-weakening friction. *Geophys. J. Int.* **173,** 674–692 (2008).
11. Melosh, H. J. Dynamical weakening of faults by acoustic fluidization. *Nature* **279,** 601–606 (1996).
12. Di Toro, G., Hirose, T., Nielsen, S., Pennacchioni, G. & Shimamoto, T. Natural and experimental evidence of melt lubrication of faults during earthquakes. *Science* **311,** 647–649 (2006).
13. Wibberley, C. A. J. & Shimamoto, T. Earthquake slip weakening and asperities explained by thermal pressurization. *Nature* **436,** 689–692 (2005).
14. Boutareaud, S. *et al.* Clay-clast aggregates: A new textural evidence for seismic fault sliding? *Geophys. Res. Lett.* **35,** L05302, doi:10.1029/2007GL032554 (2008).
15. Scholz, C. H. *The Mechanics of Earthquakes and Faulting* 2nd edn, 1–508 (Cambridge University Press, 2002).
16. Carpenter, B. M., Marone, C. & Saffer, D. Frictional behavior of materials in the 3D SAFOD volume. *Geophys. Res. Lett.* **36,** L05302, doi:10.1029/2008GL036660 (2009).
17. Vrolijk, P. & van der Pluijm, B. A. Clay gouge. *J. Struct. Geol.* **21,** 1039–1048 (1999).
18. Faulkner, D. R., Lewis, A. C. & Rutter, E. H. On the internal structure and mechanics of large strike-slip faults: field observations from the Carboneras fault, southeastern Spain. *Tectonophysics* **367,** 235–251 (2003).
19. Jefferies, S. P. *et al.* The nature and importance of phyllonite development in crustal-scale fault cores: an example from the Median Tectonic Line, Japan. *J. Struct. Geol.* **28,** 220–235 (2006).
20. Scholz, C. H. Evidence for a strong San Andreas fault. *Geology* **28,** 163–166 (2000).
21. Townend, J. & Zoback, M. D. How faulting keeps the crust strong. *Geology* **28,** 399–402 (2000).
22. Collettini, C. & Sibson, R. H. Normal faults, normal friction? *Geology* **29,** 927–930 (2001).
23. Noda, H., Dunham, E. M. & Rice, J. R. Earthquake ruptures with thermal weakening and the operation of major faults at low overall stress levels. *J. Geophys. Res.* **114,** B07302, doi:10.1029/2008JB006143 (2009).
24. Collettini, C., Viti, C., Smith, S. A. F. & Holdsworth, R. E. The development of interconnected talc networks and weakening of continental low-angle normal faults. *Geology* **37,** 567–570 (2009).
25. Beeler, N. M., Tullis, T. E., Blanpied, M. L., &. Weeks, J. D. Frictional behavior of large displacement experimental faults. *J. Geophys. Res.* **101,** 8697–8715 (1996).
26. Marone, C. Laboratory-derived friction laws and their application to seismic faulting. *Annu. Rev. Earth Planet. Sci.* **26,** 643–696 (1998).
27. Evans, J. P. & Chester, F. M. Fluid rock interaction in faults of the San Andreas system: inferences from San Gabriel fault-rock geochemistry and microstructures. *J. Geophys. Res.* **100,** 13007–13020 (1995).
28. Bos, B., Peach, C. J. & Spiers, C. J. Frictional-viscous flow of simulated fault gouge caused by the combined effects of phyllosilicates and pressure solution. *Tectonophysics* **327,** 173–194 (2000).
29. Niemeijer, A. R. & Spiers, C. J. Velocity dependence of strength and healing behaviour in simulated phyllosilicate-bearing fault gouge. *Tectonophysics* **427,** 231–253 (2006).
30. Imber, J. *et al.* in *The Internal Structure of Fault Zones: Implications for Mechanical and Fluid-Flow Properties* (eds Wibberley, C. A. J. *et al.*) Vol. 299, 151–173 (Geological Society of London Special Publication, 2008).
31. Niemeijer, A. R. & Spiers, C. J. A microphysical model for strong velocity weakening in phyllosilicate-bearing fault gouges. *J. Geophys. Res.* **112,** B10405, doi:10.1029/2007JB005008 (2007).
32. Saffer, D. M., Frye, K. F., Marone, C. & Mair, K. Laboratory results indicating complex and potentially unstable frictional behavior of smectite clay. *Geophys. Res. Lett.* **28,** 2297–2300 (2001).
33. Shea, W. T. J. & Kronenberg, A. K. Strength and anisotropy of foliated rocks with varied mica contents. *J. Struct. Geol.* **15,** 1097–1121 (1993).

Supplementary Information is linked to the online version of the paper at www.nature.com/nature.

Acknowledgements We thank I. Faoro for cutting the samples and J. P. Ampuero, D. Faulkner, R. Holdsworth and S. Smith for discussions. This research was motivated in part by stimulating discussions with P. Montone, M. Barchi and M. Cocco. We gratefully acknowledge funding by NSF grants OCE-0196462 EAR-0510182 and an INGV-DPC S5 M. Barchi grant. A.N. was supported in part by the ERC St. G. Nr.205175 USEMS project.

Author Contributions C.C., A.N. and C.M. designed the study. A.N. and C.C. carried out the experiments. A.N., C.C. and C.M. conducted the data analysis. C.C. and C.V. carried out the microstructural studies. C.V. did TEM and mineralogical characterization. All the authors contributed to the writing.

Author Information Reprints and permissions information is available at www.nature.com/reprints. Correspondence and requests for materials should be addressed to C.C. (colle@unipg.it).

METHODS

We chose rock samples from two highly foliated domains of the Zuccale fault (L2 and L3 in Fig. 1). Mineral abundances in selected fault rocks have been determined by coupling XRPD and TG-MS. For each sample, we collected three different XRPD patterns from:
(1) powders (grain size $<150\,\mu m$), representative of the bulk sample mineralogy (massive carbonate fragments + foliation);
(2) fine fraction (grain size $<2\,\mu m$, oriented samples), representative of the fine-grained foliation;
(3) fine fractions after glycolation, to distinguish expandable versus not-expandable clays.

The XRPD patterns on fine fractions revealed smectite, tremolite and talc as the main minerals within the foliation (Supplementary Fig. 1). The relative amounts of smectite, talc and tremolite, as reported in Table 1, were determined on the basis of XRPD intensity ratios. The total amount of calcite in the bulk samples was determined by TG-MS. The TG-MS data indicated that calcite decomposition occurred in the temperature range 600–800 °C. From the weight losses registered in this temperature range, we determined total calcite contents of 43% and 39% in L2 and L3, respectively.

For the experiments we collected blocks of cohesive foliated fault rocks pertaining to L2 and L3 domains and we cut them to form wafers 0.8–1.2 cm thick and 5 cm × 5 cm in area. The wafers were oriented so that they could be sheared in their *in situ* orientation, with foliation parallel to shear direction. We refer to these as solid experiments. We also carried out experiments on powders obtained from crushing and sieving ($<150\,\mu m$): (1) intact pieces of fault rock and (2) the samples used in the solid experiments. With this approach we directly compare the frictional properties of foliated fault rocks and their powdered equivalents, which have identical mineralogical compositions (Table 1). We found no difference between experiments conducted on layers of powdered fault rock and powders from solid experiments.

Experiments were conducted in a double direct shear geometry using a servo-controlled biaxial deformation apparatus[16,26] (Fig. 2a inset). Three steel blocks sandwiched two layers of fault rock while the horizontal hydraulic ram, in load feedback mode, applied normal load to the layers. The vertical ram was advanced in displacement feedback mode at constant velocity, thereby shearing the two fault rock layers. Both normal and shear loads were measured by load cells at the load point with a precision of 0.1 kN. Displacement of the horizontal and vertical axes was measured using displacement transducers with 0.1 μm precision. The sheared layers were initially 0.8–1.2 cm thick (solid fault rock) or 0.6 cm thick (powders) and we measured changes in layer thickness continuously during shear. Frictional contact area is constant during shear. Loads and displacements were continuously recorded for each axis at 10 kHz and averaged to rates from 1 to 100 Hz, depending on the sliding velocity. Normal and shear stresses were obtained by dividing the measured applied loads by the contact area of the forcing block (5 × 5 cm) in the case of normal stress, and twice the contact area in the case of shear stress.